

**DIAGNOSTIC FEATURES OF DIELECTRIC BREAKDOWN IN NATURAL SILICATES.** M. L. MacLeod<sup>1,2</sup>, T. G. Sharp<sup>2</sup>, and A. P. Jordan<sup>1</sup>, <sup>1</sup>EOS Space Science Center, University of New Hampshire, Durham, NH, USA (first author email: Morgan.MacLeod@UNH.edu), <sup>2</sup>School of Earth and Space Exploration, Arizona State University, Tempe, AZ, USA.

**Introduction:** Dielectric breakdown caused by solar energetic particle (SEP)-induced internal charging is theorized to occur in minerals on the lunar surface and other airless bodies in the Solar System [1-4]. The resulting damage to regolith grains may significantly contribute to space weathering and thus play an important role in optical maturation.

Although dielectric breakdown has been well documented as the source of anomalies in insulating spacecraft components, its microstructural and chemical effects in lunar-relevant materials have not been experimentally investigated, except in several limited studies [3, 5, 6]. Additionally, evidence of breakdown has not been identified in any extraterrestrial materials.

To better understand the effects of dielectric breakdown in natural silicate minerals, we have experimentally irradiated minerals to induce dielectric breakdown. The resulting damage has been characterized as a function of mineralogy and we have identified diagnostic features that can be used for the identification of dielectric breakdown weathering in extraterrestrial samples.

**Experimental Methods:** The effects of dielectric breakdown were characterized in four gem-quality, single-crystal silicates including an iron-rich olivine ( $\text{Mg}_{0.77}\text{Fe}_{0.23}\text{SiO}_4$ ), San Carlos olivine ( $\text{Mg}_{0.90}\text{Fe}_{0.10}\text{SiO}_4$ ), diopside, and bytownite ( $\text{An}_{72}$ ) to characterize the effects of surface and subsurface breakdown as a function of chemical composition.

Hand-polished mineral sections with thicknesses of 1 mm were electron irradiated under a defocused beam in an FEI NOVA 200 NanoLab Field Emission Scanning Electron Microscope (FE-SEM). The beam was rastered across areas  $\sim 5.66 \times 10^4 \text{ um}^2$  and  $4.60 \times 10^3 \text{ um}^2$ . The electron beam energy was 30 keV for all experimental runs, giving a maximum electron depth range of  $5.5 \text{ }\mu\text{m}$  [7]. Parameters including the beam current, scan area, and scan duration were independently adjusted to control the total supplied fluence.

Post-irradiation, secondary electron images of surface damage were taken with the NOVA 200. FIB sections of bytownite, diopside, and San Carlos olivine were prepared for transmission electron microscope (TEM) imaging using a ThermoScientific Helios 5UX FE-SEM/FIB. TEM images were acquired with an aberration-corrected FEI Titan 300/80. To minimize beam damage, the microscope was operated at 300 kV.

**Results:** Bytownite, diopside, and San Carlos olivine ( $\text{Fo}_{90}$ ) were modified to varying degrees by electrical discharging from 30-keV electron irradiation, requiring minimum fluences of  $\sim 10^{13}$ - $10^{14}$  particles  $\text{cm}^{-2}$ . The iron-rich olivine ( $\text{Fo}_{77}$ ) did not experience discharge. Two independent electrical phenomena were detected: flashovers and subsurface discharges. Each phenomenon produced plasma channels bound within the dielectric volume, liberated from the subsurface to the surface-vacuum interface, or propagated laterally along mineral surfaces.

**Flashovers.** Flashovers result from excessive surface charging. Consequently, the principal damage is the formation of “tree” structures: primary and secondary filamentous, erosional channels ( $<180 \text{ nm}$  width,  $<90 \text{ }\mu\text{m}$  length) that propagate along the surface with fractal geometries (Fig. 1). The high pressure and temperature of ionization caused material in contact with the plasma to sublime and melt. Much of this material was redeposited as thin ( $<50 \text{ nm}$ ), amorphous vapor deposits and as melt spherules  $<300 \text{ nm}$  diameter. Melt spherules were significantly iron-depleted, but no nanophase iron ( $\text{npFe}^0$ ) deposits were found.

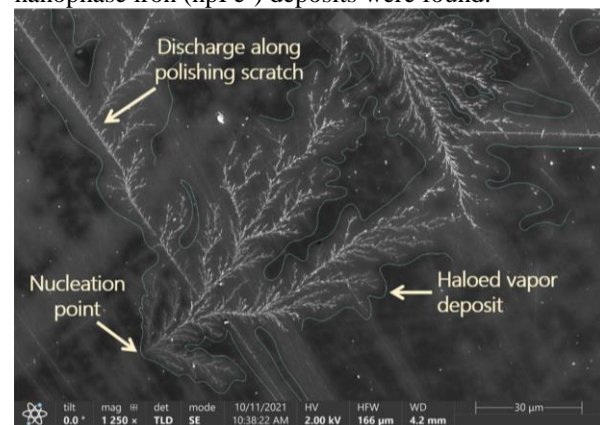


Figure 1. Flashover channels along the surface of bytownite.

**Deep dielectric breakdown.** Electrical discharges in the subsurface produced channels that were filled with amorphous material, melted by the high temperature and pressure of plasma propagation (Fig. 2). The length of subsurface channels ranged from 100s of nm to  $>3 \text{ }\mu\text{m}$ . Their widths were variable, but typically less than  $300 \text{ nm}$  at their widest points. Some discharges occurring within  $2.5 \text{ }\mu\text{m}$  of the surface erupted through the sample surface and produced pits with diameters  $<750 \text{ nm}$ .

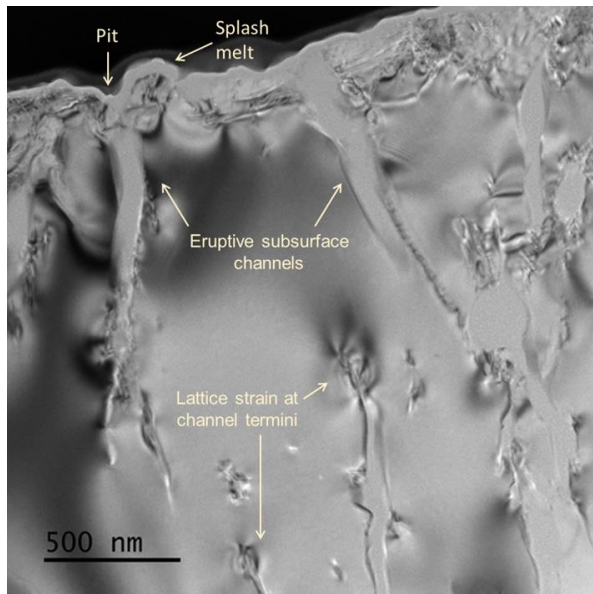


Figure 2. Characteristic subsurface breakdown damage in San Carlos olivine: melt-filled channels, surface pits, and melt and vapor deposits.

**Compositional variation.** A strong, positive correlation was found between iron abundance (wt% FeO) and the minimum fluence required to initiate deep dielectric breakdown for silicates containing <25 wt% FeO (Fig. 3). The minimum fluence required for flashovers was approximately one order of magnitude less than that for subsurface discharge, but still positively correlated with iron abundance. Minimum breakdown thresholds were lower than fluences supplied by some of the larger SEP events measured by the CRaTER instrument.

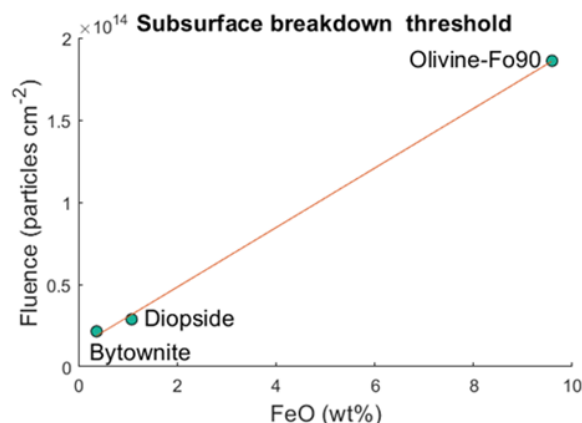


Figure 3. Minimum fluence required for subsurface dielectric breakdown as a function of iron abundance.

**Discussion:** Two electrical phenomena, subsurface discharges and flashovers, were found to occur independently and produce unique damage types. The types of damage were consistent among all phases for

fluences sufficient to cause breakdown, but the areal density of damage changes as a function of both fluence and material properties.

**Highlands vs. mare.** The correlation between conductivity (iron abundance) and the minimum fluence required to initiate breakdown has substantial implications for how breakdown weathering could affect optical signatures of the lunar surface. For a given fluence, the total number of discharge events is directly related to material conductivity and dielectric strength (minimum fluence threshold). For this reason, dielectric breakdown should occur more readily in the highlands where conductivities and charge dissipation rates are lower than the iron-rich maria. Because the sensitivity to fluence appears to be high for materials with <10 wt% FeO, there may also be differential weathering between the nearside and farside highlands.

**Permanently shadowed regions.** Because cold temperatures reduce material conductivity and increase charge dissipation rates, in permanently shadowed regions (PSRs) with temperatures below ~120 K, breakdown may occur at frequencies approximately twice that of illuminated areas at high latitudes [3]. The contribution to optical maturation in PSRs is unknown because the rate of npFe<sup>0</sup> formation by breakdown has not yet been determined. If solar wind hydrogen implantation plays an important role in the formation of npFe<sup>0</sup>, then the primary contribution of dielectric breakdown in PSRs may be comminution and increased porosity of the epiregolith.

**Conclusions:** The fluences at which dielectric breakdown occurred in these experiments suggests that large SEP events supply sufficient fluence to cause breakdown and that evidence of breakdown should be detectable in iron-deficient, lunar regolith at high latitudes. Additional work is required to determine charging and discharging behaviors in granular materials, and to determine the conditions under which dielectric breakdown can produce nanophase iron. These additional studies are required to constrain the potential contribution of dielectric breakdown weathering to optical maturation of regolith.

**References:** [1] Jordan A. P. et al. (2017) *Icarus*, 283, 352-358. [2] Jordan A. P. et al. (2018) *Adv. in Space. Res.*, 62(8), 2187-2198. [3] Jordan A. P. et al. (2019) *Icarus*, 319, 785-794. [4] Jordan A. P. (2022) *Icarus*, 376, 114878. [5] Lemelle et al. (2003) *Geochim. et Cosmochim. Acta*, 67(10), 1901-1910. [6] Izenberg N. R. et al. (2018) *LPS XLIX*, Abstract #1588. [7] Demers H. et al. (2011) *Scanning*, 33(3), 135-146.

**Acknowledgements:** This study was supported by NASA grants NNG07EK00C and NNG11PA03C.